Vietnam Journal of Science and Technology ***62*** *(6) (2024) 1196-1209*
doi:10.15625/2525-2518/19281

Size-dependent nonlinear bending of tapered cantilever microbeam based on modified couple stress theory

Bui Thi Thu Hoai[1], Le Cong Ich[2], Nguyen Dinh Kien[3, 4, *]

[1]*Faculty of Vehicle and Energy Engineering, Phenikaa University, Ha Dong, Ha Noi, Viet Nam*

[2]*Faculty of Mechanical Engineering, Le Quy Don Technical University, 236 Hoang Quoc Viet, Bac Tu Liem, Ha Noi, Viet Nam*

[3]*Institute of Mechanics, 18 Hoang Quoc Viet, Cau Giay, Ha Noi, Viet Nam*

[4]*VNU University of Engineering and Technology, 144 Xuan Thuy, Cau Giay, Ha Noi, Viet Nam*

[*]Email: *ndkien@imech.vast.vn*

Received: 27 October 2023; Accepted for publication: 30 March 2024

Abstract. A size-dependent beam formulation based on the classical beam theory and modified couple stress theory (MCST) is derived for nonlinear bending analysis of a microcantilever under an end force/moment. The microbeam is linearly tapered in the directions of width and height. The formulation is derived using the concept of the co-rotational formulation in which the vector of internal forces and tangent stiffness matrix are firstly constructed in the element-attached coordinates and then transferred to the global ones. The nonlinear response is predicted by the iterative method and the arc-length technique. The numerical investigation confirms the efficiency of the derived formulation, and it can predict accurate nonlinear responses of the microcantilever by using just several elements. The result reveals the importance of the microstructural size effects on the nonlinear responses and ignoring the size effects leads to an overestimation of the deflections. The impacts of various factors such as the scale parameter and the tapered ratio on the nonlinear behavior of the microcantilever are investigated in detail.

Keywords: Tapered microbeam, MCST, size-dependent nonlinear behavior, co-rotational approach, geometrical nonlinearity.

Classification numbers: 5.4.2, 5.4.5.

1. INTRODUCTION

Microbeams with thickness in the order of microns are widely seen in micro-electro-mechanical systems (MEMS) [1, 2]. The microbeams in these systems are often buckled and often

undergo large deflections, which motivates geometrically nonlinear analysis of microstructures, investigation that are most closed to the present topic are briefly summarized below.

The traditional beam theories were adopted in deriving the size-dependent nonlinear beam models in the early stage [3 - 6]. The von Kármán assumption is used to model deformation, and the nonlinear responses to electro-mechanical loading are assessed using the shooting method [3] or Galerkin technique [5, 6]. To model the size effects in small-scale structures, several higher-order continuum theories, e.g. the strain gradient elasticity theory (SGET) [7, 8] and modified couple stress theory (MCST) [9] were developed. Using the MCST and MSGT to model the size effect, Mohammadi and Mahzoon [10] studied postbuckling of microbeams subjected to axial force and temperature change. The static bending, post-buckling and vibration analyses of microbeams were presented in [11], showing the significance of size effect when the ratio of thickness to the length scale parameter is about one.

Non-prismatic beams are of great importance in practice because of their ability to meet architectural requirements and optimize the structural weight. Some effort has been made in nonlinear analysis of the beams with non-prismatic sections. A closed-form solution for buckling problems of columns with variable cross-section was derived in Ref. [12]. A paralinear element considering the non-uniform section was derived in [13] for computing the large displacements of columns under an eccentric axial force. Cleghorn and Tabarrok [14] used the solution of a tapered Timoshenko beam in their derivation of the property matrices for assessing vibration characteristics of non-prismatic beams. Baker [15] solved the governing equations of a tapered cantilever under distributed loads, and then determined the large deflection beam profiles. The solution in series for deflections of non-prismatic members with small displacements is derived in [16]. Lee *et al*. [17] employed Runge-Kutta method to solve the differential equations of tapered cantilevers undergoing large displacements. The deformed configurations of non-prismatic cantilevers with Ludwick material subjected to a tipping moment were determined by Brojan *et al*. [18] using an exact moment-curvature formula. The free vibration analysis of non-prismatic beams was presented in [19] by using the exact shape functions to derive the structural matrices.

In this paper, the nonlinear analysis of a micro-scale cantilever undergoing large deflections is carried out using the nonlinear finite element method. The microcantilever is considered to be linearly tapered in the directions of width and height. A co-rotational finite element is derived and employed to construct the nonlinear equilibrium equation. The formulation is formulated in the framework of the classical beam theory and the MCST accounting for the microstructural scale effect. Newton-Raphson method is employed in combination with the arc-length technique to obtain the nonlinear load-deflection curves of the microcantilever. Numerical investigations are presented to show the influence of the tapered ratio and the scale parameter on the nonlinear behavior of the tapered micro-scale cantilever beam.

2. MATERIAL AND METHOD

2.1. Co-rotational approach

Figure 1 shows a tapered micro-scale cantilever in a coordinate system (x,y,z). The microcantilever is linearly tapered in the directions of width and height according to

$$b(x) = b_0\left(1-\alpha\frac{x}{L}\right), \quad h(x) = h_0\left(1-\alpha\frac{x}{L}\right) \tag{1}$$

where L is the beam length; $b(x)$ and $h(x)$ are, respectively, the width and height of the cross-section with abscissa x; b_0 and h_0 are, respectively, the width and height of the section at the clamped end; $0 \le \alpha < 1$ is the tapered ratio.

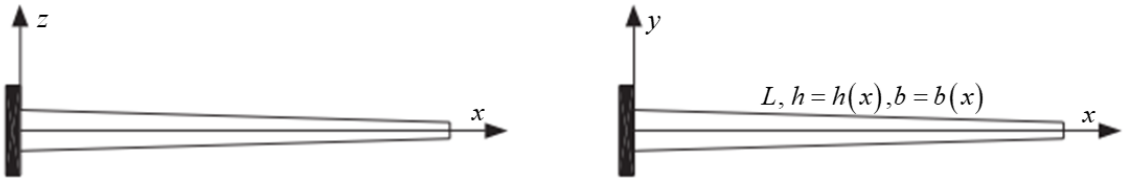

Figure 1. Tapered cantilever microbeam under investigation.

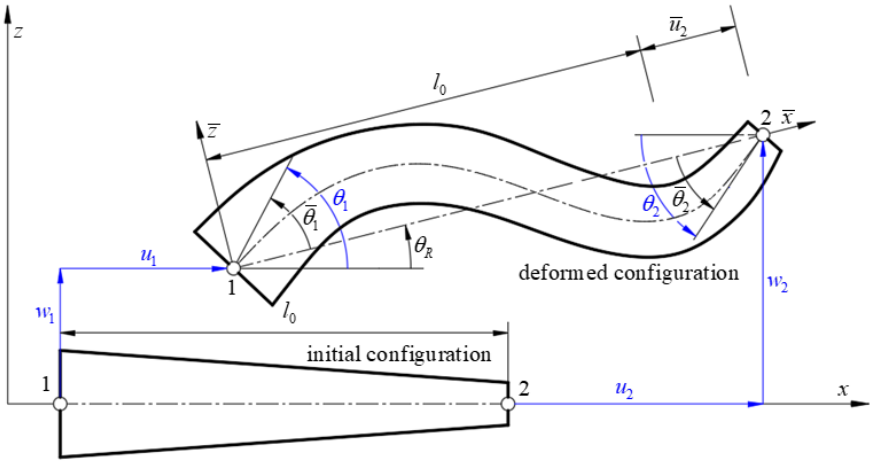

Figure 2. Co-rotational beam element with local and global degrees of freedom

Figure 2 illustrates a 2-node beam element and its degrees of freedom in two Cartesian coordinates, a local system $(\bar{x}, \bar{z})$ and a global one (x, z). The system (x, z) is fixed in space, the system $(\bar{x}, \bar{z})$ always translates and rotates with the element in the deformation process. The system $(\bar{x}, \bar{z})$ is chosen such that the origin is always at node 1, while the $\bar{x}$ - axis directs from node 1 to node 2. With the chosen local system, the local axial displacement at node 1 and the transverse displacements at both the two nodes are vanished, $\bar{u}_1 = \bar{w}_1 = \bar{w}_2 = 0$. In this regard, the element vector of degrees of freedom with respects to the local coordinates, ($\bar{\mathbf{d}}$), has the form

$$\bar{\mathbf{d}} = \left\{ \bar{u}_2 \quad \bar{\theta}_1 \quad \bar{\theta}_2 \right\}^T \tag{2}$$

In the above equation, $\bar{u}_2$ is the local displacement in $\bar{x}$ - direction at the node 2; $\bar{\theta}_1$ and $\bar{\theta}_2$ are, respectively, the rotations with respect the local coordinates at both the two nodes. In Eq. (2) and in the below, the bar suffix is used to define a variable defined in the local coordinates, and the superscript 'T' indicates the transpose of a matrix or a vector.

In general, the global degrees of freedom are nonzero, and thus the element vector of nodal displacements with respect to the global coordinates (**d**) contains six components as follows

$$\mathbf{d} = \left\{ u_1 \quad u_2 \quad w_1 \quad \theta_1 \quad w_2 \quad \theta_2 \right\}^T \tag{3}$$

with u_i, w_i, θ_i $(i=1, 2)$ are, respectively, the global axial displacement, transverse displacement and the rotation at the node *i*. The vector of nodal forces with respect to the local coordinates associated with the local vector of nodal degrees of freedom in Eq. (2) has the following forms

$$\bar{\mathbf{f}}_{\text{in}} = \left\{ \bar{f}_{\bar{u}} \quad \bar{\mathbf{f}}_{\bar{\boldsymbol{\theta}}} \right\}^T \quad \text{with} \quad \bar{f}_{\bar{u}} = \bar{N}_2, \ \bar{\mathbf{f}}_{\bar{\boldsymbol{\theta}}} = \left\{ \bar{M}_1 \quad \bar{M}_2 \right\}^T \tag{4}$$

where $\bar{N}_2$ is the local force in $\bar{x}$ - direction at the node 2; $\bar{M}_1$ is the local moment at node 1, while $\bar{M}_2$ is the local moment at node 2. The corresponding vector of global nodal forces associated with the vector of global nodal degrees of freedom in Eq. (3) is as follows

$$\mathbf{f}_{\text{in}} = \left\{ \mathbf{f}_{\mathbf{u}} \quad \mathbf{f}_{\boldsymbol{\theta}} \right\}^T, \text{ with } \mathbf{f}_{\mathbf{u}} = \left\{ N_1 \quad N_2 \right\}, \ \mathbf{f}_{\boldsymbol{\theta}} = \left\{ Q_1 \quad M_1 \quad Q_2 \quad M_2 \right\} \tag{5}$$

with N_i (i = 1, 2) is the global axial force at node *i*; Q_i and M_i are, respectively, the global shear force and moment at the nodes.

The local displacement and the rotations in Eq. (2) can be approximately calculated from the global ones in Eq. (3) by considering the geometry of Figure 2, and they have the forms

$$\bar{u}_2 = l_c - l_0, \qquad \bar{\theta}_1 = \theta_1 - \theta_R, \qquad \bar{\theta}_2 = \theta_2 - \theta_R \tag{6}$$

In Eq. (5), l_0 is the initial length of the element, while l_c is the length of the deformed element. These quantities can be computed from the nodal coordinates of the element and the current nodal degrees of freedom; θ_R is the element rigid rotation, which can be calculated as [20, 21]

$$\theta_R = \arctan\left(\frac{w_2 - w_1}{x_2 + u_2 - x_1 - u_1} \right) \tag{7}$$

where x_i (i = 1,2) is the initial abscissa of node *i*; u_i, w_i (i = 1, 2) are the axial and transverse displacements with respect to the global coordinates at node *i*, respectively.

The vector of the nodal forces and the matrix of the tangent stiffness, $\mathbf{f}_{in}$ and $\mathbf{k}_t$, respectively, can be calculated from the expression of the strain energy (U) of the element as follows

$$\mathbf{f}_{\text{in}} = \frac{\partial U}{\partial \mathbf{d}} = \frac{\partial U}{\partial \bar{\mathbf{d}}} \frac{\partial \bar{\mathbf{d}}}{\partial \mathbf{d}} = \mathbf{T}_1^T \bar{\mathbf{f}}_{\text{in}}, \ \mathbf{k}_t = \frac{\partial^2 U}{\partial \mathbf{d}^2} = \mathbf{T}_1^T \bar{\mathbf{k}}_t \mathbf{T}_1 + \bar{\mathrm{N}}_2 \mathbf{T}_2 + (\bar{\mathrm{M}}_1 + \bar{\mathrm{M}}_2) \mathbf{T}_3 \tag{8}$$

where $\bar{\mathbf{f}}_{\text{in}} = \dfrac{\partial U}{\partial \bar{\mathbf{d}}}$ and $\bar{\mathbf{k}}_t = \dfrac{\partial^2 U}{\partial \bar{\mathbf{d}}^2}$ are, respectively, the vector of the nodal forces and the matrix of tangent stiffness with respect to the local coordinates; $\mathbf{T}_1$, $\mathbf{T}_2$ and $\mathbf{T}_3$ are the transformation matrices, and they can be computed from the local and global relations in Eq. (6) as follows

$$\mathbf{T}_1 = \frac{\partial \bar{\mathbf{d}}}{\partial \mathbf{d}}, \ \mathbf{T}_2 = \frac{\partial^2 \bar{u}_2}{\partial \mathbf{d}^2}, \ \mathbf{T}_3 = -\frac{\partial^2 \theta_R}{\partial \mathbf{d}^2} \tag{9}$$

The vector of the nodal forces $\mathbf{f}_{in}$ and the tangent stiffness matrix $\mathbf{k}_t$ are defined by Eqs. (8) and (9) in case the vector $\bar{\mathbf{f}}_{\text{in}}$ and the matrix $\bar{\mathbf{k}}_t$ are known, and thus the global formulation is defined.

2.2. Size-dependent local formulation

According to the classical beam theory, the displacements $\bar{u}$ and $\bar{w}$ of a point inside the element in the $\bar{x}$ - and $\bar{z}$ -directions are

$$\bar{u}(\bar{x},\bar{z}) = \bar{u}_0(\bar{x}) - \bar{z}\,\bar{\theta}(\bar{x}), \qquad \bar{w}(\bar{x},\bar{z}) = \bar{w}_0(\bar{x}) \tag{10}$$

with $\bar{u}_0(\bar{x})$ and $\bar{w}_0(\bar{x})$ respectively denote the local axial and the transverse displacement of a point on the $\bar{x}$-axis, and $\bar{\theta} = \partial\bar{w}_0/\partial\bar{x}$ is the local rotation of cross section.

The following shallow arch formulation can be adopted for the local normal strain in the large displacement analysis of the micro-scale beam [20]

$$\bar{\varepsilon}_{\bar{x}}(\bar{x},\bar{z}) = \bar{u}_{0,\bar{x}}(\bar{x}) + \frac{1}{2}\bar{w}_{0,\bar{x}}^2 - \bar{z}\,\bar{\theta}_{,\bar{x}}(\bar{x}) = \bar{\varepsilon}_0(\bar{x}) - \bar{z}\,\bar{w}_{0,\bar{x}\bar{x}}(\bar{x}), \tag{11}$$

where $\bar{\varepsilon}_0(\bar{x}) = \bar{u}_{0,\bar{x}}(\bar{x}) + \frac{1}{2}\bar{w}_{0,\bar{x}}^2$ is the membrane strain. The subscript comma in Eq. (11) and in the below denotes the derivative with respect to the variable that follows, e.g. $\bar{w}_{0,\bar{x}} = \partial\bar{w}_0/\partial\bar{x}$.

Assuming that the element material follows the Hooke's law, the normal stress $(\bar{\sigma}_x)$ is related to the normal strain in Eq. (11) by

$$\bar{\sigma}_{\bar{x}}(\bar{x},\bar{z}) = E\,\bar{\varepsilon}_{\bar{x}}(\bar{x},\bar{z}) = E(\bar{\varepsilon}_0 - \bar{z}\,\bar{w}_{0,\bar{x}\bar{x}}), \tag{12}$$

where E is the elastic modulus.

The axial displacement $\bar{u}_0$ and the transverse displacement $\bar{w}_0$ with respect to the $(\bar{x},\bar{z})$ system are respectively interpolated from their nodal values by linear and cubic polynomials as follows

$$\bar{u}_0 = \bar{h}_{\bar{u}}\bar{u}_2, \;\; \bar{w}_0 = \bar{\mathbf{h}}_{\bar{w}}\bar{\boldsymbol{\theta}} \tag{13}$$

where $\bar{\boldsymbol{\theta}} = \left\{\bar{\theta}_1, \quad \bar{\theta}_2\right\}^T$ and

$$\bar{h}_{\bar{u}} = \frac{\bar{x}}{l_0}, \;\; \bar{\mathbf{h}}_{\bar{w}} = \left\{\bar{x} - \frac{2\bar{x}^2}{l_0} + \frac{\bar{x}^3}{l_0^2}, \quad -\frac{\bar{x}^2}{l_0} + \frac{\bar{x}^3}{l_0^2}\right\} \tag{14}$$

It should be noted that Eqs. (13) and (14) have been written in regard to that $\bar{u}_1 = \bar{w}_1 = \bar{w}_2 = 0$. Differentiating of $\bar{u}_0$ and $\bar{w}_0$ in (13) with respect to $\bar{x}$, one gets

$$\bar{u}_{0,\bar{x}} = \bar{b}_{\bar{u}}\bar{u}_2, \;\; \bar{w}_{0,\bar{x}} = \bar{\mathbf{b}}_{\bar{w}}\bar{\boldsymbol{\theta}}, \;\; \bar{w}_{0,\bar{x}\bar{x}} = \bar{\mathbf{c}}_{\bar{w}}\bar{\boldsymbol{\theta}} \tag{15}$$

where

$$\begin{aligned} \bar{b}_{\bar{u}} = \bar{h}_{\bar{u},\bar{x}} = \frac{1}{l_0}, \;\; \bar{\mathbf{b}}_{\bar{w}} = \bar{\mathbf{h}}_{\bar{w},\bar{x}} = \left\{1 - \frac{4\bar{x}}{l_0} + \frac{3\bar{x}^2}{l_0^2}, \quad -\frac{2\bar{x}}{l_0} + \frac{3\bar{x}^2}{l_0^2}\right\} \\ \bar{\mathbf{c}}_{\bar{w}} = \bar{\mathbf{b}}_{\bar{w},\bar{x}} = \left\{-\frac{4}{l_0} + \frac{6\bar{x}}{l_0^2}, \quad -\frac{2}{l_0} + \frac{6\bar{x}}{l_0^2}\right\} \end{aligned} \tag{16}$$

Because of the membrane locking problem, the normal strain in Eq. (11) and the interpolating functions (14) cannot be used directly to generate the vector of local internal forces and local matrix of tangent stiffness. To avoid this problem, the membrane strain $\bar{\varepsilon}_0$ in (11) is replaced by the following effective strain [20]

$$\bar{\varepsilon}_{\text{eff.}} = \frac{1}{l_0}\int_0^{l_0}\bar{\varepsilon}_0 \mathrm{d}\bar{x} = \frac{1}{l_0}\int_0^{l_0}\left(\bar{u}_{0,\bar{x}} + \frac{1}{2}\bar{w}_{0,\bar{x}}^2\right)\mathrm{d}\bar{x} \tag{17}$$

Using Eqs. (13), (14) and (15), one can express Eq. (17) in the following form

$$\bar{\varepsilon}_{\text{eff.}} = \bar{b}_{\bar{u}}\bar{u}_2 + \frac{1}{2l_0}\bar{\boldsymbol{\theta}}^T\left(\int_0^{l_0}\bar{\mathbf{b}}_{\bar{w}}^T\bar{\mathbf{b}}_{\bar{w}}\mathrm{d}\bar{x}\right)\bar{\boldsymbol{\theta}} = \bar{b}_{\bar{u}}\bar{u}_2 + \bar{\boldsymbol{\theta}}^T\,\bar{\mathbf{B}}\,\bar{\boldsymbol{\theta}} \tag{18}$$

where

$$\bar{\mathbf{B}} = \frac{1}{2l_0}\int_0^{l_0}\bar{\mathbf{b}}_{\bar{w}}^T\bar{\mathbf{b}}_{\bar{w}}\mathrm{d}\bar{x} = \frac{1}{60}\begin{bmatrix} 4 & -1 \\ -1 & 4 \end{bmatrix} \tag{19}$$

Since the classical structural theories cannot model the microstructural size effects of micro-scale structures, the MCST with only one additional material length scale parameter in [9] is employed herein to evaluate the elastic energy of the micro-scale beam element as

$$U = \frac{1}{2}\int_V\left(\bar{\boldsymbol{\sigma}}:\bar{\boldsymbol{\varepsilon}} + \bar{\mathbf{m}}:\bar{\boldsymbol{\chi}}\right)\mathrm{d}V = \frac{1}{2}\int_0^{l_0}\int_A\left(\bar{\boldsymbol{\sigma}}:\bar{\boldsymbol{\varepsilon}} + \bar{\mathbf{m}}:\bar{\boldsymbol{\chi}}\right)\mathrm{d}A\mathrm{d}\bar{x} \tag{20}$$

In the above equation, V denotes the element volume; $\bar{\boldsymbol{\sigma}}$ is the stress tensor; $\bar{\boldsymbol{\varepsilon}}$ is the strain tensor; $\bar{\mathbf{m}}$ is the deviatoric part of the couple stress tensor, and $\bar{\boldsymbol{\chi}}$ is the symmetric tensor of curvatures. These tensors have the following form [9]

$$\bar{\boldsymbol{\sigma}} = \lambda\,\mathrm{tr}(\bar{\boldsymbol{\varepsilon}})\mathbf{I} + 2\mu\,\bar{\boldsymbol{\varepsilon}},\ \bar{\boldsymbol{\varepsilon}} = \frac{1}{2}\left[\nabla\bar{\mathbf{u}} + (\nabla\bar{\mathbf{u}})^T\right],\ \bar{\boldsymbol{\chi}} = \frac{1}{2}\left[\nabla\bar{\boldsymbol{\beta}} + (\nabla\bar{\boldsymbol{\beta}})^T\right],\ \bar{\mathbf{m}} = 2l^2\mu\,\bar{\boldsymbol{\chi}} \tag{21}$$

with l denotes the material length scale parameter; λ and μ are Láme coefficients defined as

$$\lambda = \frac{E\nu}{(1+\nu)(1-2\nu)},\ \mu = \frac{E}{2(1+\nu)} \tag{22}$$

where ν is the Poisson's ratio; μ is also the shear modulus; $\bar{\boldsymbol{\beta}}$ and $\bar{\mathbf{u}}$ are, respectively, the vectors of rotations and displacements with the following form

$$\bar{\boldsymbol{\beta}} = \mathrm{curl}(\bar{\mathbf{u}}),\ \bar{\mathbf{u}} = \left\{\bar{u},\quad 0,\quad \bar{w}\right\}^T \tag{23}$$

with the classical beam theory adopted herein, the vector of rotations in (23) has the form

$$\bar{\boldsymbol{\beta}} = \left\{0,\quad -\bar{w}_{0,\bar{x}},\quad 0\right\}^T \tag{24}$$

using Eq. (24), one can express the $\bar{\boldsymbol{\chi}}$ and $\bar{\mathbf{m}}$ in (21) in the form

$$\bar{\boldsymbol{\chi}} = -\frac{1}{2}\begin{bmatrix} 0 & \bar{w}_{0,\bar{x}\bar{x}} & 0 \\ \bar{w}_{0,\bar{x}\bar{x}} & 0 & 0 \\ 0 & 0 & 0 \end{bmatrix},\ \bar{\mathbf{m}} = -l^2\mu\begin{bmatrix} 0 & \bar{w}_{0,\bar{x}\bar{x}} & 0 \\ \bar{w}_{0,\bar{x}\bar{x}} & 0 & 0 \\ 0 & 0 & 0 \end{bmatrix} \tag{25}$$

The tensors of stresses and strains tensors in the classical beam theory have the following simple form

$$\bar{\boldsymbol{\sigma}} = \begin{bmatrix} \bar{\sigma}_{\bar{x}} & 0 & 0 \\ 0 & 0 & 0 \\ 0 & 0 & 0 \end{bmatrix},\quad \bar{\boldsymbol{\varepsilon}} = \begin{bmatrix} \bar{\varepsilon}_{\bar{x}} & 0 & 0 \\ 0 & 0 & 0 \\ 0 & 0 & 0 \end{bmatrix} \tag{26}$$

Using Eqs. (25) and (26), one can recast the elastic energy for the element in (20) in the following form

$$U=\frac{1}{2}\int_0^{l_0}\int_{-b/2}^{b/2}\int_{-h/2}^{h/2}\left(\bar{\boldsymbol{\sigma}}:\bar{\boldsymbol{\varepsilon}}+\bar{\mathbf{m}}:\bar{\boldsymbol{\chi}}\right)\mathrm{d}\bar{z}\,\mathrm{d}\bar{y}\,\mathrm{d}\bar{x}=\frac{1}{2}\int_0^{l_0}\int_{-b/2}^{b/2}\int_{-h/2}^{h/2}\left(\bar{\sigma}_x\bar{\varepsilon}_x+l^2\mu\, w_{0,xx}^2\right)\mathrm{d}\bar{z}\,\mathrm{d}\bar{y}\,\mathrm{d}\bar{x} \tag{27}$$

where

$$b=b_0\left(1-\alpha\frac{\bar{x}_0+\bar{x}}{L}\right),\ h=h_0\left(1-\alpha\frac{\bar{x}_0+\bar{x}}{L}\right),\ 0\le\bar{x}\le l_0 \tag{28}$$

with $\bar{x}_0$ is the abscissa with respect to the beam left end to the 1st node.

Substituting Eqs. (11)-(18) and (25) into Eq. (27) leads to

$$U=\frac{1}{2}\int_0^{l_0}\Big[EA\left((\bar{\boldsymbol{\theta}}^T\bar{\mathbf{B}}\bar{\boldsymbol{\theta}})^2+2(\bar{\boldsymbol{\theta}}^T\bar{\mathbf{B}}\bar{\boldsymbol{\theta}})(\bar{b}_{\bar{u}}\bar{u}_2)+(\bar{b}_{\bar{u}}\bar{u}_2)^2\right)+EI(\bar{\mathbf{c}}_{\bar{w}}\bar{\boldsymbol{\theta}})^2+l^2\mu A(\bar{\mathbf{c}}_{\bar{w}}\bar{\boldsymbol{\theta}})^2\Big]\mathrm{d}\bar{x} \tag{29}$$

In the above equation, A and I denote the area and second-order moment of inertia of the cross-section at $\bar{x}$, respectively, which can be expressed as

$$A=b_0h_0\left(1-\alpha\frac{\bar{x}_0+\bar{x}}{L}\right)^2,\ I=\frac{b_0h_0^3}{12}\left(1-\alpha\frac{\bar{x}_0+\bar{x}}{L}\right)^4 \tag{30}$$

The vector of local internal forces $\bar{\mathbf{f}}_{\text{in}}$ is obtained by differentiation of the elastic energy (29) with respect to the local degrees of freedom as

$$\begin{aligned}
\bar{f}_{\bar{u}}&=\frac{\partial U}{\partial\bar{u}_2}=\int_0^{l_0}EA\bar{b}_{\bar{u}}(\bar{\boldsymbol{\theta}}^T\bar{\mathbf{B}}\bar{\boldsymbol{\theta}}+\bar{b}_{\bar{u}}\bar{u}_2)\mathrm{d}\bar{x}=E\hat{A}\bar{b}_{\bar{u}}(\bar{\boldsymbol{\theta}}^T\bar{\mathbf{B}}\bar{\boldsymbol{\theta}}+\bar{b}_{\bar{u}}\bar{u}_2)\\
\underset{(2\times2)}{\bar{\mathbf{f}}_{\bar{\boldsymbol{\theta}}}}&=\frac{\partial U}{\partial\bar{\boldsymbol{\theta}}}=\int_0^{l_0}\left(EI+l^2\mu A\right)(\bar{\mathbf{c}}_{\bar{w}}^T\bar{\mathbf{c}}_{\bar{w}})\bar{\boldsymbol{\theta}}\mathrm{d}\bar{x}+2\int_0^{l_0}EA\bar{b}_{\bar{u}}\left(\bar{\boldsymbol{\theta}}^T\bar{\mathbf{B}}\bar{\boldsymbol{\theta}}+\bar{b}_{\bar{u}}\bar{u}_2\right)(\bar{\mathbf{B}}\bar{\boldsymbol{\theta}})\mathrm{d}\bar{x}\\
&=\left(E\hat{\mathbf{C}}_1+l^2\mu\hat{\mathbf{C}}_2\right)\bar{\boldsymbol{\theta}}+2E\hat{A}\bar{b}_{\bar{u}}\left(\bar{\boldsymbol{\theta}}^T\bar{\mathbf{B}}\bar{\boldsymbol{\theta}}+\bar{b}_{\bar{u}}\bar{u}_2\right)(\bar{\mathbf{B}}\bar{\boldsymbol{\theta}})
\end{aligned} \tag{31}$$

with

$$\hat{A}=\int_0^{l_0}A\mathrm{d}\bar{x},\quad \hat{\mathbf{C}}_1=\int_0^{l_0}I(\bar{\mathbf{c}}_{\bar{w}}^T\bar{\mathbf{c}}_{\bar{w}})\mathrm{d}\bar{x},\quad \hat{\mathbf{C}}_2=\int_0^{l_0}A(\bar{\mathbf{c}}_{\bar{w}}^T\bar{\mathbf{c}}_{\bar{w}})\mathrm{d}\bar{x} \tag{32}$$

The local matrix $\bar{\mathbf{k}}_t$ can be split into sub-matrices as

$$\underset{(3\times3)}{\bar{\mathbf{k}}_t}=\begin{bmatrix}\bar{k}_{\bar{u}\bar{u}} & \bar{\mathbf{k}}_{\bar{u}\bar{\boldsymbol{\theta}}}\\ \bar{\mathbf{k}}_{\bar{u}\bar{\boldsymbol{\theta}}}^T & \bar{\mathbf{k}}_{\bar{\boldsymbol{\theta}}\bar{\boldsymbol{\theta}}}\end{bmatrix} \tag{33}$$

where the sub-matrices have the form

$$\begin{aligned}
\bar{k}_{\bar{u}\bar{u}}&=\frac{\partial\bar{f}_{\bar{u}}}{\partial\bar{u}_2}=E\hat{A}\bar{b}_{\bar{u}}^2,\ \underset{(1\times2)}{\bar{\mathbf{k}}_{\bar{u}\bar{\boldsymbol{\theta}}}}=\frac{\partial\bar{f}_{\bar{u}}}{\partial\bar{\boldsymbol{\theta}}}=2E\hat{A}\bar{b}_{\bar{u}}(\bar{\boldsymbol{\theta}}^T\bar{\mathbf{B}})\\
\underset{(2\times2)}{\bar{\mathbf{k}}_{\bar{\boldsymbol{\theta}}\bar{\boldsymbol{\theta}}}}&=\frac{\partial\bar{\mathbf{f}}_{\bar{\boldsymbol{\theta}}}}{\partial\bar{\boldsymbol{\theta}}}=2E\hat{A}\bar{b}_{\bar{u}}\left(3\bar{\boldsymbol{\theta}}^T\bar{\mathbf{B}}\bar{\boldsymbol{\theta}}+\bar{b}_{\bar{u}}\bar{u}_2\right)\bar{\mathbf{B}}+\left(E\hat{\mathbf{C}}_1+l^2\mu\hat{\mathbf{C}}_2\right)
\end{aligned} \tag{34}$$

Having the vector of local internal forces $\bar{\mathbf{f}}_{\text{in}}$ and the matrix of tangent stiffness $\bar{\mathbf{k}}_t$ derived, the element formulation is completely defined by Eqs. (8) and (9).

2.3. Numerical algorithm

The derived vector of element forces $\mathbf{f}_{\text{in}}$ and the matrix of tangent stiffness $\mathbf{k}_t$ are assembled into the global vector and matrix to form the equilibrium equation for the microcantilever, which can be written in the form [21], [22]

$$\mathbf{g}(\mathbf{p},\lambda_L)=\mathbf{q}_{in}(\mathbf{p})-\lambda_L\mathbf{q}_{ef}=0 \tag{35}$$

where $\mathbf{p}$ and $\mathbf{q}_{in}$ are the global vectors of degrees of freedom and internal forces at the nodes, respectively; $\mathbf{q}_{ef}$ is the vector of fixed external load, and λ_L is the scalar loading parameter. The vector $\mathbf{g}$ in (35) is named as out of balance force vector.

The arc-length technique in [22] is employed herewith to handle the complex situations, e.g. the snap-through and snap-back. This technique considers the loading parameter λ_L as an additional unknown, and the following constraint equation is introduced

$$a=\left(\Delta\mathbf{p}^T\Delta\mathbf{p}+\Delta\lambda_L\psi\mathbf{q}_{ef}^T\mathbf{q}_{ef}\right)-\Delta l_{sc}^2=0 \tag{36}$$

where ψ is the scaling parameter, and Δl_{sc} is a fixed arc length. The nodal displacements and the loading parameter can be obtained from Eqs. (35) and (36) by the Newton-Raphson iterative method. The arc-length technique and its implementation are given in details in [20], [22]

A converge criterion is needed for the iterative method. In the present work, a criterion based on the Euclidean norm of the out of balance force vector adopted as

$$\|\mathbf{g}\|\le\varepsilon\left\|\lambda_L\mathbf{q}_{ef}\right\| \tag{37}$$

with ε is the tolerance, taken by 10^{-4} for all numerical example in Section 3.

3. NUMERICAL INVESTIGATION

The nonlinear response of the tapered microcantilever to a concentrated load/moment at the free end is predicted in this section. The following non-dimensional parameters are introduced for the tip displacements, the length scale parameter and external load

$$\hat{u}=\frac{u_L}{L},\ \hat{w}=\frac{w_L}{L},\quad \hat{\theta}=\frac{\theta_L}{(\pi/2)},\quad \eta=\frac{l}{h_0},\ \hat{P}=\frac{PL^2}{EI_0},\ \hat{M}=\frac{ML}{EI_0} \tag{38}$$

where u_L, and w_L are, respectively, the tip displacements in x and z directions; θ_L is the tip rotation; P and M are the concentrated load and moment acting at the free end, respectively; I_0 is the moment of inertia of the clamped section. Otherwise stated, a beam made of steel with $E=210$ GPa, $\nu=0.3$ and a ratio $L/h_0=50$ is employed in the below.

3.1. Formulation verification

Because no data on the large deformation of microcantilever are found by the authors in the literature, a macro-scale cantilever beam made of steel, previously studied by Lee *et al*. in Ref. [17], is considered. The cantilever is linearly tapered in the width direction, $b(x)=b_0\left(1-\alpha x/L\right)$, and with a ratio $I_0/I_L=3$ (α = 2/3). The non-dimensional parameters for the external loads are [17]: $\hat{P}=PL^2/(EI_L)$ and $\hat{M}=ML/(EI_L)$, with I_L as the moment of inertia of the tip. Table 1 compares the tip normalized responses of the tapered cantilever beam under a combination of the tip load and moment obtained by the present formulation with the results of Ref. [17]. One can see from the table that the displacements and rotation obtained by the present formulation

agree very well with that of Ref. [17], where the classical beam theory and Runge-Kutta method have been employed. It is noted that the results in Table 1 are obtained by using six elements, and no improvement is seen by using more than six elements.

Table 1. Comparison of tip responses of a macro-scale tapered cantilever under a combination of transverse tip load and tip.

$\hat{P}$	$\hat{M}$	Present				Ref. [17]		
		$\lvert\hat{u}\rvert$	$\hat{w}$	$\hat{\theta}$		$\lvert\hat{u}\rvert$	$\hat{w}$	$\hat{\theta}$
5	0	0.1670	0.4918	0.5408		0.1678	0.4926	0.5428
0	2	0.1411	0.4137	0.6994		0.1411	0.4136	0.6994
5	2	0.3635	0.6429	1.0085		0.3640	0.6433	0.9969

To verify the ability of the element in bending analysis of microbeam, Table 2 compares the dimensionless maximum linear deflection of a pinned-pinned (PP) uniform microbeam subjected to uniform distributed load q_0 obtained herein with the results of Ref. [23]. In the reference, various beam theories are used to analyze the linear bending problem. The result in the table is obtained by present formulation by deleting the nonlinear terms. The deflections in Table 2 are given for various values of η, and the following data: E = 427 (MPa), υ = 0.17, L/h = 10, b = h. Good agreement between the maximum deflections obtained by the present formulation with that of Ref. [23] is noted from Table 2, irrespective of the scale parameter. Noting that the scale parameter in Table 2 is defined in accordance with the cited reference.

Table 2. Comparison of the maximum deflection ($\bar{w} = 100 w_{\max} E_0 I / q_0 L^4$, $I = bh^3/12$ $E_0 = 70\,\text{GPa}$) for PP microbeam with linear bending model.

Source	Theories	η = 0	η = 1	η = 1/2	η = 1/4	η =1/ 8
Ref. [23]	Classical Beam Theory	0.2133	0.0348	0.0935	0.1616	0.1976
	First-order Beam Theory	0.2181	0.0364	0.096	0.1653	0.2021
	Third-order Beam Theory (TBT)	0.2181	0.0352	0.0949	0.1647	0.2018
	Sinusoidal Beam Theory (STB)	0.2181	0.0352	0.0949	0.1647	0.2018
	Quasi-3D TBT	0.2179	0.0352	0.0949	0.1646	0.2016
	Quasi-3D SBT	0.2178	0.0352	0.0949	0.1646	0.2016
Present	Classical Beam Theory	0.2135	0.0348	0.0935	0.1616	0.1976

3.2. Microbeam under a tip transverse load

The tapered microcantilever subjected to a transverse tip load P is analyzed. In Table 3, the non-dimensional tip displacements of the microbeam corresponding to $\hat{P} = 5$ are given for some values of the tapered ratio α and the non-dimensional scale parameter η. The significant influence of the tapered ratio and the size-scale effect on the nonlinear behavior of the microbeam can be seen clearly in the table. The increase of the tapered ratio increases the tip displacements, while they are decreased when increasing the non-dimensional scale parameter η. Thus, ignoring the size effect leads to an overestimation of the tip displacements of the microcantilever.

The influence of the tapered ratio and the size scale parameter on the nonlinear behavior of the tapered micro-scale cantilever beam can also be seen from Figure 3, where the curves of load-displacement relation of the microcantilever are depicted for several values of the non-dimensional scale parameter η and the tapered ratio α. At a given transverse load, as can be seen from Figure 3a, the increase of the scale parameter results in a decrease of the tip displacements, while, as expected, the increase of the tapered ratio results in the increase of the tip response (Figure 3b). The different influence of the scale parameter and the tapered ratio on the nonlinear response of the microcantilever can also be seen in Figure 4, where the deformed configurations of the microbeam are depicted for several values of the non-dimensional size-scale parameter and the tapered ratio. The result obtained in this sub-section confirms the important role of the size-scale parameter on the nonlinear response of the micro-scale beam and the tip displacements of the microcantilever are considerably underestimated when ignoring the micro-scale size effect. It is noted that the numerical result in this sub-section is convergence by six elements also.

Table 3. Tip normalized displacements of tapered microbeam corresponding to $\hat{P} = 5$ for different tapered ratios and dimensionless scale parameters.

α	Response	η				
		0	0.25	0.50	0.75	1.00
0.0	$\lvert\hat{u}\rvert$	0.3876	0.3209	0.1928	0.0963	0.0461
	$\hat{w}$	0.7139	0.6636	0.5355	0.3896	0.2737
0.1	$\lvert\hat{u}\rvert$	0.4105	0.3428	0.2101	0.1068	0.0516
	$\hat{w}$	0.7233	0.6759	0.5523	0.4067	0.2877
0.2	$\lvert\hat{u}\rvert$	0.4338	0.3656	0.2289	0.1188	0.0582
	$\hat{w}$	0.7314	0.6870	0.5689	0.4247	0.3029
0.3	$\lvert\hat{u}\rvert$	0.4570	0.3888	0.2492	0.1326	0.0660
	$\hat{w}$	0.7380	0.6967	0.5850	0.4435	0.3197
0.4	$\lvert\hat{u}\rvert$	0.4799	0.4122	0.2710	0.1484	0.0754
	$\hat{w}$	0.7433	0.7049	0.6002	0.4631	0.3381
0.5	$\lvert\hat{u}\rvert$	0.5018	0.4353	0.2942	0.1667	0.0869
	$\hat{w}$	0.7476	0.7117	0.6143	0.4831	0.3583

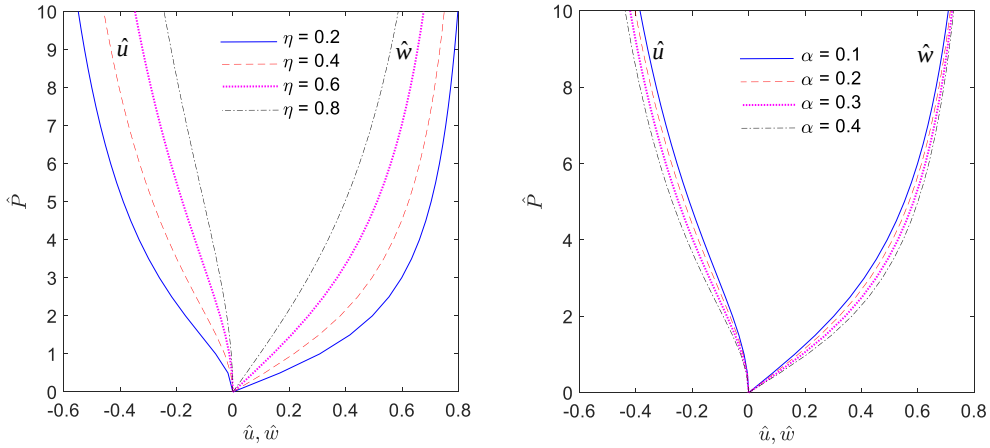

a) $\alpha = 0.2$ b) $\eta = 0.5$

Figure 3. Load-displacement curves of tapered microcantilever subjected to tip load for different dimensionless scale parameters and tapered ratios.

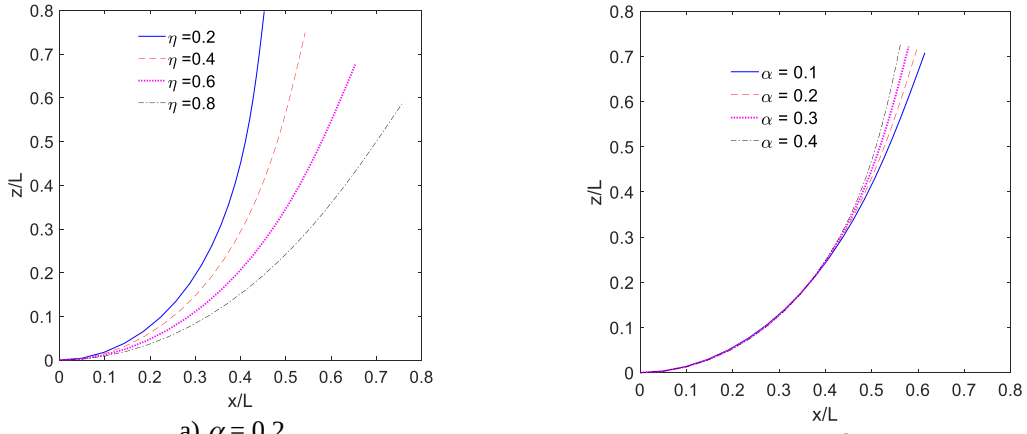

a) $\alpha = 0.2$ b) $\eta = 0.5$

Figure 4. Deformed configurations of microcantilever under tip load corresponding to $\hat{P} = 10$ for different non-dimensional scale parameters and tapered ratios.

3.3. Roll-up of microcantilever by end moment

Roll-up of a tapered microcantilever due to a moment *M* acting at the free end is studied in this sub-section. In Table 4, the non-dimensional tip displacements of the microcantilever corresponding to $\hat{M} = 1.2$ are listed for several values of the tapered ratio and the size-scale parameter. Similar to the case of the microcantilever under the tip transverse load, an increase in the tapered ratio leads to an increase in the tip displacements. On the other hand, the response of the microcantilever is more conservative when the micro-size effect is taken into consideration, and this tendency is more pronounced for the microcantilever with a higher scale parameter.

Table 4. Tip normalized displacements of tapered microcantilever corresponding to $\hat{M} = 1.2$ for different tapered ratios and size-scale parameter.

α	Response	η				
		0	0.25	0.50	0.75	1.00
0.0	$\lvert\hat{u}\rvert$	0.2233	0.1384	0.0509	0.0185	0.0076
	$\hat{w}$	0.5314	0.4330	0.2714	0.1653	0.1064
0.1	$\lvert\hat{u}\rvert$	0.2972	0.1802	0.0638	0.0225	0.0091
	$\hat{w}$	0.5793	0.4768	0.2982	0.1802	0.1154
0.2	$\lvert\hat{u}\rvert$	0.4040	0.2402	0.0815	0.0280	0.0112
	$\hat{w}$	0.6178	0.5233	0.3294	0.1978	0.1260
0.3	$\lvert\hat{u}\rvert$	0.5517	0.3271	0.1068	0.0356	0.0140
	$\hat{w}$	0.6189	0.5657	0.3657	0.2188	0.1387
0.4	$\lvert\hat{u}\rvert$	0.7120	0.4494	0.1437	0.0465	0.0179
	$\hat{w}$	0.5691	0.5851	0.4072	0.2442	0.1543
0.5	$\lvert\hat{u}\rvert$	0.7318	0.5977	0.1993	0.0630	0.0239
	$\hat{w}$	0.5078	0.5504	0.4518	0.2755	0.1738

The effects of the size-scale parameter and the tapered ratio on the behavior of the microbeam can also be seen clearly in Figure 5 and Figure 6, where the curves of load-displacement relation and the deformed configurations are respectively illustrated for several values of the scale parameter and tapered ratio. An increase in the size-scale parameter leads to a decrease in the tip displacements (Figure 5a), while the tip response of the microcantilever increases by increasing the tapered ratio (Figure 5b).

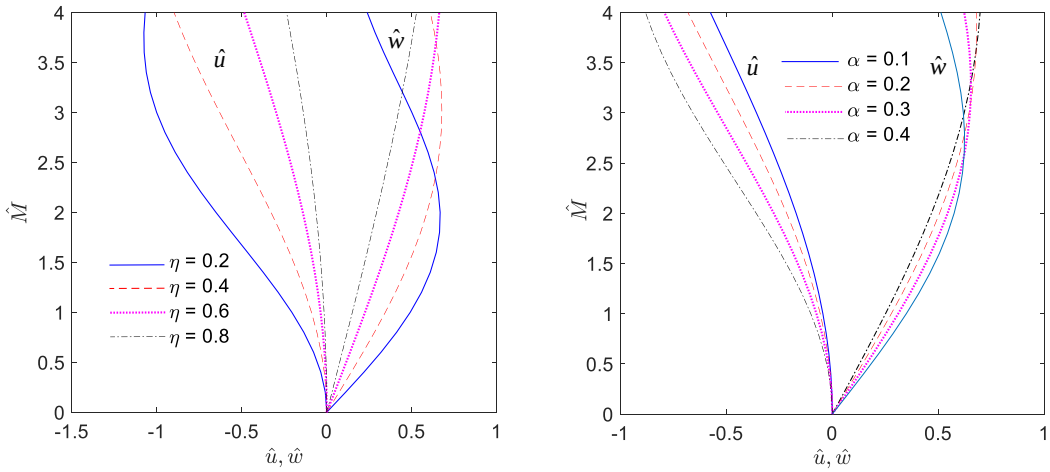

a) $\alpha = 0.2$ b) $\eta = 0.5$

Figure 5. Load-displacement curves of tapered microcantilever under tip moment for different dimensionless size-scale parameters and tapered ratios.

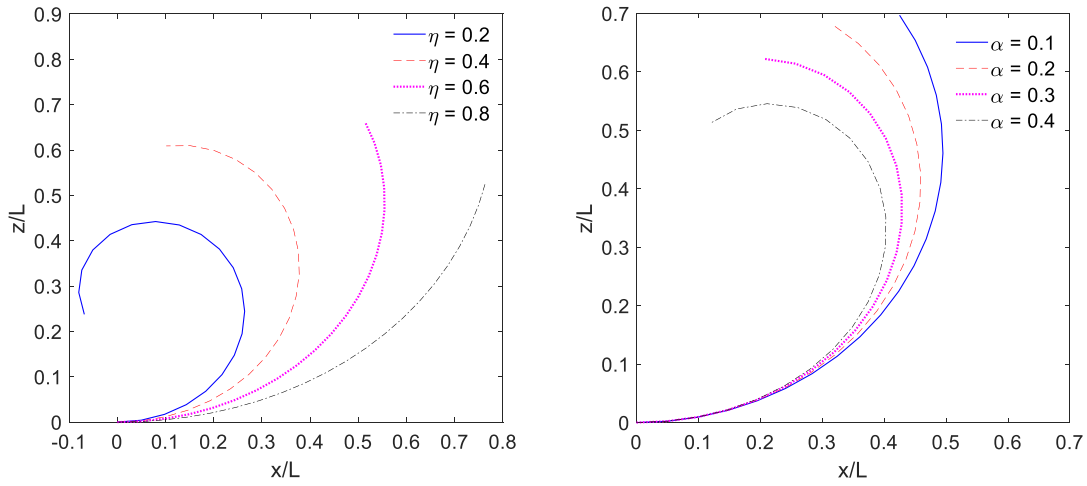

a) $\alpha = 0.2$ b) $\eta = 0.5$

Figure 6. Deformed configurations of cantilever microcantilever corresponding to $\hat{M} = 4$ for various values of dimensionless size-scale parameter and tapered ratio.

The deformed configurations of the microbeam corresponding to $\hat{M} = 4$ as illustrated in Figure 6 for different non-dimensional size-scale parameters and tapered ratios also confirm the impacts of the size effect and the tapered ratio on the nonlinear response of the tapered microcantilever. The microcantilever is more conservative when it is associated with a higher size-scale parameter (Fig. 6a), while it is more flexible by increasing the taper ratio (Fig. 6b).

4. CONCLUSIONS

The size-dependent nonlinear behavior of a micro-scale tapered cantilever beam was studied using a co-rotational element. The MCST was employed with the classical beam theory to derive the vector of internal forces and the matrix of tangent stiffness. Newton-Raphson's iterative method was adopted with the arc-length technique to solve the nonlinear equation and to compute the equilibrium paths. The impacts of the tapered ratio and the size-scale parameter on the nonlinear response of the microcantilever under a tip transverse load/end moment have been investigated in detail. The numerical result has confirmed that the derived formulation is efficient, and it can predict accurately large deflections of the microbeam by using a small number of elements. The obtained result also reveals that the influence of the size-scale parameter and the tapered ratio on the nonlinear response of the microcantilever is opposite. While the increase of the tapered ratio enhances the tip displacement response of the microcantilever, the nonlinear response is more conservative by considering the microstructural size effect, and this is more pronounced for a microcantilever having a higher material length scale parameter.

Acknowledgements. The work presented in this article was supported by Vietnam National Foundation for Science and Technology Development (NAFOSTED), grant number 107.02-2021.11.

CRediT authorship contribution statement. Bui Thi Thu Hoai: Formal analysis, Data curation Visualization. Le Cong Ich: Methodology, Investigation, Formal analysis, Validation, Writing - original draft. Nguyen Dinh Kien: Conceptualization, Supervision, Writing - review & editing, Funding acquisition.

Declaration of competing interest. The authors declare that they have no known competing financial interests or personal relationships that could have appeared to influence the work reported in this paper.

REFERENCES

1. Faris W., Nayfeh A. H. - Mechanical response of a capacitive microsensor under thermal load, Communications in Nonlinear Science and Numerical Simulation **12** (5) (2007) 776-783. https://doi.org/10.1016/j.cnsns.2005.06.006.
2. Thai H. T., Vo T. P., Nguyen T. K., Kim S. E. - A review of continuum mechanics models for size-dependent analysis of beams and plates, Composite Structures **177** (2017) 196-219. https://doi.org/10.1016/j.compstruct.2017.06.040.
3. Collenz A., De Bona F., Gugliotta A. Somà A. - Large deflections of microbeams under electrostatic loads, Journal of Micromechanics and Microengineering **14** (3) (2003) 365. https://DOI 10.1088/0960-1317/14/3/008.
4. Abdel-Rahman E. M., Younis M. I., Nayfeh A. H. - Characterization of the mechanical behavior of an electrically actuated microbeam, Journal of Micromechanics and Microengineering **12** (6) (2002) 759-766. https://doi.org/10.1088/0960-1317/12/6/306.
5. Abdel-Rahman E. M., Nayfeh A. H. - Secondary resonances of electrically actuated resonant microsensors, Journal of Micromechanics and Microengineering **13** (3) (2003) 491-501. https://doi.org/10.1088/0960-1317/13/3/320.
6. Younis M. I. - Multi-mode excitation of a clamped–clamped microbeam resonator, Nonlinear Dynamics **80** (3) (2015) 1531-1541. https://doi.org/10.1007/s11071-015-1960-1.
7. Lam D. C. C., Yang F., Chong A. C. M., Wang J., Tong P. - Experiments and theory in strain gradient elasticity. Journal of the Mechanics and Physics of Solids **51**(8) (2003) 1477–1508. https://doi.org/10.1016/S0022-5096(03)00053-X.
8. Zhao J., Zhou S., Wang B., Wang X. - Nonlinear microbeam model based on strain gradient theory, Applied Mathematical Modelling **36** (6) (2012) 2674-2686. https://doi.org/10.1016/j.apm.2011.09.051
9. Yang F. A. C. M., Chong A. C. M., Lam D. C. C., Tong P. - Couple stress based strain gradient theory for elasticity, International Journal of Solids and Structures **39** (10) (2002) 2731-2743. https://doi.org/10.1016/S0020-7683(02)00152-X.
10. Mohammadi H., Mahzoon M. - Thermal effects on postbuckling of nonlinear microbeams based on the modified strain gradient theory, Composite Structures **106** (2013) 764-776. https://doi.org/10.1016/j.compstruct.2013.06.030.
11. W. Xia, L. Wang, and L. Yin - Nonlinear non-classical microscale beams: static bending, postbuckling and free vibration, International Journal of Engineering Science **48** (12) (2010) 2044-2053. https://doi.org/10.1016/j.ijengsci.2010.04.010.
12. Timoshenko S. P., Gere J. M. - Theory of elastic stability, New York: McGraw-Hill, 1961. https://doi.org/10.1017/S0368393100104389
13. Wood R. D., Zienkiewicz O. C. - Geometrically nonlinear finite element analysis of beams, frames, arches and axisymmetric shells, Comput Struct **7** (6) (1977) 725-735. https://doi.org/10.1016/0045-7949(77)90027-X
14. Cleghorn W. L., Tabarrok B. - Finite element formulation of a tapered Timoshenko beams for free lateral vibration analysis, J Sound Vib. **152** (3) (1992) 461-470. https://doi.org/10.1016/0022-460X(92)90481-C

15. Baker G. - On the large deflections of non-prismatic cantilevers with a finite depth, Comput Struct. **46** (2) (1993) 365-370. https://doi.org/10.1016/0045-7949(93)90201-N
16. Baker G. - Exact deflections in non-prismatic beam members, Comput Struct. **61** (3) (1996) 515-528. https://doi.org/10.1016/0045-7949(96)00046-6
17. Lee B. K., Wilson J. F., Oh S. J. - Elastica of cantilevered beams with variable cross section, Int. J. Non-Linear Mech. **28** (5) (1993) 579-589. https://doi.org/10.1016/0020-7462(93)90049-Q
18. Brojan M., Videnic T., Kosel F. - Large deflections of nonlinearly elastic nonprismatic cantilever beams made from materials obeying the generalized Ludwick law, Meccanica **44** (6) (2009) 733-739. https://doi.org/10.1007/s11012-009-9209-z
19. Attarnejad R., Semnani S. J., Shahba A. - Basic displacement functions for free vibration analysis of non- prismatic Timoshenko beams, Finite Elem. Anal. Des. **46**(10) (2010) 916–929. https://doi.org/10.1016/j.finel.2010.06.005
20. Crisfield M. A. - Nonlinear finite element analysis of solids and structures. Volume 1: Essentials, Wiley, New York, 1991. https://www.osti.gov/biblio/226942
21. Nguyen D. K. - Large displacement response of tapered cantilever beams made of axially functionally graded material, Composites Part B: Engineering **55** (2013) 298-305. https://doi.org/10.1016/j.compositesb.2013.06.024
22. Crisfield M. A. - A fast incremental/iterative solution procedure that handles "snapthrough", Computers & Structures **13** (1981) 55-62. https://doi.org/10.1016/00457949(81)90108-5
23. Trinh L. C., Nguyen H. X., Vo T. P., Nguyen T. K. - Size-dependent behaviour of functionally graded microbeams using various shear deformation theories based on the modified couple stress theory, Composite Structures **154** (2016) 556-572. https://doi.org/10.1016/j.compstruct.2016.07.033